Vol 16 No 2, February 2007
1009-1963/2007/16(02)/0485-08

Chinese Physics

© 2007 Chin. Phys. Soc.
and IOP Publishing Ltd

# Simulation of radio-frequency atmospheric pressure glow discharge in $\gamma$ mode*

Shang Wan-Li(尚万里)[a], Wang De-Zhen(王德真)[a]†, and Michael G. Kong[b]

[a] *State Key Laboratory of Materials Modification by Laser, Ion and Electron Beams, Department of Physics, Dalian University of Technology, Dalian* 116024, *China*

[b] *Department of Electronic and Electrical Engineering, Loughborough University, Leicestershire LE11 3TU, U.K.*

(Received 8 April 2006; revised manuscript received 9 August 2006)

The existence of two different discharge modes has been verified in an rf (radio-frequency) atmospheric pressure glow discharge (APGD) by Shi [*J. Appl. Phys.* **97**, 023306 (2005)]. In the first mode, referred to as $\alpha$ mode, the discharge current density is relatively low and the bulk plasma electrons acquire the energy due to the sheath expansion. In the second mode, termed $\gamma$ mode, the discharge current density is relatively high, the secondary electrons emitted by cathode under ion bombardment in the cathode sheath region play an important role in sustaining the discharge. In this paper, a one-dimensional self-consistent fluid model for rf APGDs is used to simulate the discharge mechanisms in the $\gamma$ mode in helium discharge between two parallel metallic planar electrodes. The results show that as the applied voltage increases, the discharge current becomes greater and the plasma density correspondingly increases, consequentially the discharge transits from the $\alpha$ mode into the $\gamma$ mode. The high collisionality of the APGD plasma results in significant drop of discharge potential across the sheath region, and the electron Joule heating and the electron collisional energy loss reach their maxima in the region. The validity of the simulation is checked with the available experimental and numerical data.

**Keywords:** radio-frequency atmospheric pressure glow discharge, plasma simulation
**PACC:** 5280, 5270, 5220

## 1. Introduction

Plasmas have been used for material treatment in a number of fields, such as surface activation, etching, cleaning, decontamination, and thin film coating.[1,2] Industrial plasmas operate either at a low pressure ($< 2.6 \times 10^2$ Pa) or at atmospheric pressure.[3] Capacitive discharges, inductively coupled plasma, and electron cyclotron resonance plasma sources normally work at low pressures.[2,4] Atmospheric pressure discharges fall into two main categories: thermal plasma torches, which exhibit gas temperature exceeding 3000 °C,[5,6] and nonequilibrium discharges, which run at near room temperature.[7,8] There are limitations in application of torches to substrates that are not thermally sensitive,[3] and in addition they require high voltage and high current to maintain the discharge.[9,10] Dielectric barrier discharges can produce nonequilibrium plasmas at atmospheric pressure.[3] These devices are powered by high frequency supplies operating up to 20 kHz.[7,8]

Also, atmospheric pressure glow discharges (APGDs) can work at low gas temperatures, typically below 300 °C (with the exception of microhollow cathode discharge and the surface-wave discharge), and provide reasonable reaction rates for etching, ashing, and deposition over limited areas.[11] They have recently attracted much attention, because they work at atmospheric pressure, they are not necessarily equipped with a vacuum chamber that is indispensable for low-pressure glow discharges, thereby they are expected to have many applications.[12−17] APGD can provide capacitive nonthermal plasmas generated between two parallel planar electrodes that are either metallic[18,19] or coated with a dielectric layer,[16,20] and their generation has been achieved in a very wide frequency spectrum ranging from dc,[19,21] through kHz[16,20] and MHz,[18,22] to microwave.[23] They can also be generated as surface-wave discharge.[24] Furthermore, it is indicated that these sources may produce discharges that resemble low pressure glow discharges and share some of the merits of the low pres-

*Project supported by the National Natural Science Foundation of China(Grant Nos 50528707 and 50537020).
†E-mail: wangdez@dlut.edu.cn

sure plasma sources.[11−14] On the other hand, rf capacitive discharges at intermediate pressures ($1\times10^3-2\times10^4$ Pa) have been used extensively since the advent of high power gas lasers in the 1980 s, such as $CO_2$ lasers.[25−28] Today the APGDs are found to have wide-ranging applications including etching, deposition, surface modification, and sterilization.[16,17]

A self-consistent fluid model of radio-frequency glow discharge has been used to prove the existence of two different discharge regimes at low pressures.[29] However, most experimental[30] and computational studies[31] reported so far suggest that rf APGD may operate only in a regime of low current density and a significant increase in current density tends to evolve the discharge directly into an arc plasma, thus bypassing the $\gamma$ mode of the large current density commonly seen in medium pressure glow discharges.[28] It is reported that there are also two regimes in the progress of APGD, indicated in both simulation[32] and experiment.[33] The rough characteristics about the $\gamma$ mode of the atmospheric pressure radio-frequency capacitive glow discharge is described,[32] and to further investigate the specific mechanism involved in this mode, a theoretical study is preferred since it allows for access to many important physical quantities. In this paper, a fluid model of rf APGDs in helium discharge between two metallic parallel planar electrodes is constructed on the basis of the continuity equations, the current conservation law, and the electron energy balance equation in order to study the discharge mechanism. A higher plasma density and much stronger discharge current density, as well as greater mean electron energy, are observed than for their counterparts of the numerical simulation in Ref.[31]. It is also displayed that the secondary electron emission plays an important role in the $\gamma$ mode discharge.

## 2. Model

Various configurations of electrodes are used in APGDs; the planar configuration is the most simple and suitable for the theoretical description.[34] In our numerical model, two metallic parallel planar electrodes are used. The model of discharge in helium must contain at least three species, they are molecular ions $He_2^+$, metastable atoms $He^*$ and molecules $He_2^*$.[35] It is not necessary to take the metastable state $2^1S$ into account particularly, since its behaviour is the same as that of the lowest metastable state $2^3S$.[35] In this paper, the equations are solved for a total density of these two metastable states. There are six species considered in our model, namely, electrons e, helium ions $He^+$, metastable helium atoms $He^*$, helium molecule ions $He_2^+$, metastable helium molecules $He_2^*$, and background helium atoms He, which are identical with those used in Ref.[31]. This model includes several reactions among these species, the rates are shown in Table 1.

**Table 1.** The elementary processes in pure helium.

| Process | Notation | $\Delta E$/eV | Rate coefficient/(cm$^3$/s) | Reference |
|---|---|---|---|---|
| Direct ionization | $He+e \rightarrow He^+ +2e$ | 24.6 | | [36] |
| Excitation | $He+e \rightarrow He^* +e$ | 20.215 | $4.2\times10^{-9}Te^{0.31}e^{-19.8/T_e}$ | [37] |
| Transit of resonance atoms | $He^* + 2He \rightarrow He_2^* + He$ | | $1.3\times10^{-33}$ | [31] |
| Change transfer | $He^+ + 2He \rightarrow He_2^+ + He$ | | $2.0\times10^{-31}$ | [37] |
| Stepwise ionization | $He^* + 2He^* \rightarrow e + He + He^+$ | −15.0 | $8.7\times10^{-10}$ | [38] |
| Recombination | $He^+ + e \rightarrow He$ | | $n_e 1.327\times10^{-21}(T_e/T_g)^{-4.4}$ | [39] |
| | $He_2^+ + e \rightarrow 2He$ | | $4.0\times10^{-9}$ | [40] |
| Resonance ionization | $He^* + e \rightarrow He^+ +2e$ | 4.365 | $1.28\times10^{-7}T_e^{0.6}e^{-4.78/T_e}$ | [37] |
| De-excitation | $He^* + e \rightarrow He+e$ | −20.215 | $2.9\times10^{-9}$ | [38] |
| Dissociative recombination | $He_2^+ + e \rightarrow He^* + He$ | | $5.9\times10^{-9}$ | [40] |

The simulation of the rf APGD is based on the one-dimensional continuity equations for electrons, ions, metastable atoms and molecules, with the much simpler current conservation law replacing the Poisson equation for electric field, so that the solution would automatically obey the Poisson equation and the electron energy conservation equation for the electron mean energy. The equations are given as follows:

$$\frac{\partial n_{e,i,*}}{\partial t} + \frac{\partial j_{e,i,*}}{\partial x} = S_{e,i,*}, \tag{1}$$

$$\frac{\partial E}{\partial t} + \frac{e}{\varepsilon_0} j_c = \frac{e}{\varepsilon_0} j_0, \quad (2)$$

$$\frac{\partial}{\partial t}\left(\frac{3}{2} k T_e n_e\right) + \frac{\partial q_e}{\partial x} + e j_e E + p_{coll} = 0, \quad (3)$$

where $n$ and $j$ are the density and flow density of species, $S$ represents sources and losses of particles due to the reactions, the subscripts e, i, and * denote respectively electrons, ions and metastable species. $E$ is the longitudinal electric field, $j_c$ the conduction current density, and $j_0$ the total current density. $\varepsilon_0$ represents the permittivity of vacuum, $k$ the Boltzmann constant, $T_c$ the electron temperature, and $p_{coll}$ the energy losses in various reactions. $q_e$ is the electron thermal flow, given by

$$q_e = -K_e \frac{\partial T_e}{\partial x} + \frac{5}{2} k T_e j_e, \quad (4)$$

where

$$K_e = \frac{3}{2} k D_e n_e. \quad (5)$$

The flow densities are as follows:

$$j_{e,i} = \mp \mu_{e,i} n_{e,i} - D_{e,i} \frac{\partial n_{e,i}}{\partial x}, \quad (6)$$

$$j_* = -D_* \frac{\partial n_*}{\partial x}, \quad (7)$$

where $D$ is the diffusion coefficient and $\mu$ is the mobility. The potential waveform between electrodes is given and assumed to be of the form

$$V = V_{rf} \sin(\omega t). \quad (8)$$

The density and temperature of the neutral background gas are assumed to be constant in time and uniform in space. This assumption implies that the densities of the excited and charged species stay small compared with the density of the background gas, so that pressure gradients can be neglected.[41]

The secondary electron emission effect at the cathode surface is considered as follows:

$$j_e = -\gamma \sum_i j_i, \quad (9)$$

where $\gamma$ is the secondary emission coefficient.

# 3. Results

### A. The comparison of the results from our model with the experimental data

In order to check the validation of our model, the direct comparison between available data[30,31] and our simulation results for $V - I$ characteristics of the discharge has been performed. A 13.56 MHz APGD is performed in a helium–nitrogen mixture at $8 \times 10^4$ Pa, with their electrode gap fixed at 2.4 mm, and without secondary electron emission effect taken into account.[31] The gas temperature is assumed to be 393 K. All these parameters applied in our mode are to compare our simulated $V - I$ relationship with the available experimental data[30] and numerical data[31] under the same operation conditions. The nitrogen content is set at 5 ppm that is the same as that in Ref.[30]. As shown in Fig.1, the numerical data agree with the experimental and numerical results in general. The main effect of the impurity can significantly cause a decrease in differential impedance of the discharge as compared with that in pure helium discharge.[31] Practically, if some amount of nitrogen is added the nitrogen molecules react with the metastable species, thereby greatly increasing the density of charged particles, i.e. the discharge current density, and reduce the breakdown voltage. Therefore, Fig.1 suggests that our plasma model is capable of accurately capturing the main features of rf APGDs and is reliable for the study of their operation models. The reactions and rates about the impurity are identical with those used in Ref.[42].

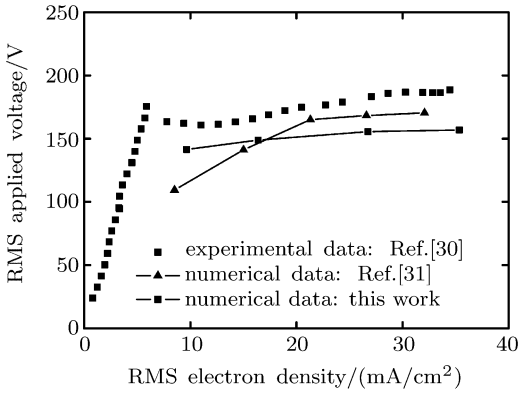



**Fig.1.** Comparison of the voltage–current relationship predicted by our model with available data from Refs.[30, 31] where RMS stands for root-mean-square.

### B. Two operation regimes

To investigate the discharge characteristics of $\gamma$ mode in rf APGDs, a pure helium discharge is operated at $1.0 \times 10^5$ Pa. The gap between two electrodes is 2 mm and rf frequency is 13.56 MHz, with

the gas temperature assumed to be room temperature (300 K). It is mentioned that the secondary electron emission plays an important role in rf APGDs.[32] The emission coefficient is 0.05 in our model.

In order to analyse the discharge in the $\gamma$ mode, a description of the transition of the two modes in our simulation is needed. The plasma density (referring to the density in the central region of the electrodes) *vs* voltage amplitude is presented to validate the two modes of rf APGD.[32] In this paper another curve is given to distinguish between these two modes. Figure 2 shows the variation of the discharge current density amplitude as a function of rf voltage amplitude. In this figure there exist two different regions that can be distinguished between according to the slope of the discharge current density amplitude as a function of the potential amplitude. When the voltage is below 434 V, the current density increases slowly at a rate of about 0.807 mA/V as the voltage amplitude increases, after that the rate changes to 6.333 mA/V, which is 8.220 times bigger. It seems that the 434 V is the transition point that divides the discharge into two modes. So, similar to the simulation of medium pressure glow discharge[29] and APGD,[32] the regime below 434 V with a slowly plasma density increasing rate is $\alpha$ mode, and the abruptly changing phase is the so-called $\gamma$ mode. The fundamental difference between the two regimes is related to the discharge sustaining mechanism.

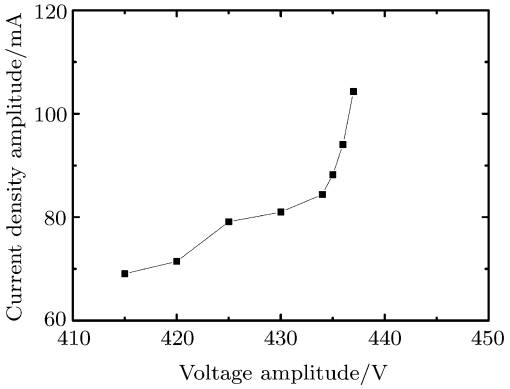



**Fig.2.** Variation of the plasma density as a function of the rf voltage amplitude.

### C. Discharge characteristics of $\gamma$ mode

The applied voltage and discharge current density as a function of time in a steady state are shown in Fig.3 for a $1.0 \times 10^5$Pa discharge with a 2-mm inter-electrode spacing and an applied voltage amplitude of 436 V. The current density amplitude is calculated to be about 95 mA/cm$^2$. The waveforms show a smooth and near-sinusoidal current characteristic for the sinusoidal voltage applied. The voltage lags behind the total current in phase by 38.8°, which also indicates the completely capacitive feature of our discharge. This capacitive component is formed by the capacitance between the two metallic planar electrodes. The resistive component arising from the ionized gas results in the shift in phase. These results are similar to the numerical data in Ref.[31], as far as the curve shape is concerned.

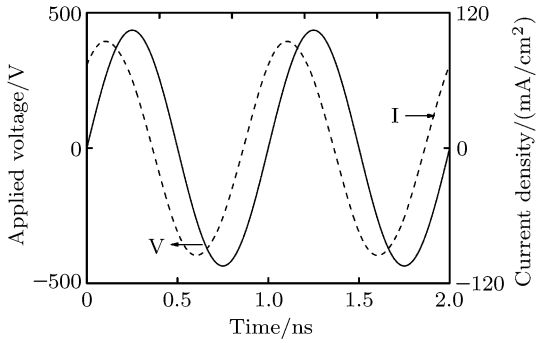



**Fig.3.** Voltage and current density waveforms at a voltage amplitude of 436 V in the $\gamma$ mode.

Figure 4 shows the time variations of the total current density and its different components (ion, electron, and displacement) on the left electrode. In the first mode, the ion current density is comparatively weak and in the second mode the ion current density is non-negligible. As a result, there appears a stronger secondary electron flow emitted from the cathode in the $\gamma$ mode than in the $\alpha$ mode. The electrons gain the energy from the electric field in the sheath and then lose it through excitation, dissociation, and ionization of the gas molecules, developing an intense gas discharge between the two electrodes at the same time.

The displacement current density is much bigger than the electron- and ion-current densities and plays an important role in the total current density both in the $\alpha$ mode and $\gamma$ mode. Approximately the electron current is bigger than the ion current at the momentary anode, and oppositely the ion current is more important at the momentary cathode. However, the ion current is much greater than electron current in the first $0.2\,T$ where $T$ is the period of the applied voltage, which may be caused by the delay due to the resistance of the discharge gas. As can be seen, the displacement current density decreases abruptly and changes its sign, and the electron current is dominant from $0.2\,T$ to $0.5\,T$ in the first half-period for plasma electrons to start to flow to the momentary anode. The electron current density at the left electrode is the biggest in the whole period in this phase, which may lead to a big current density.

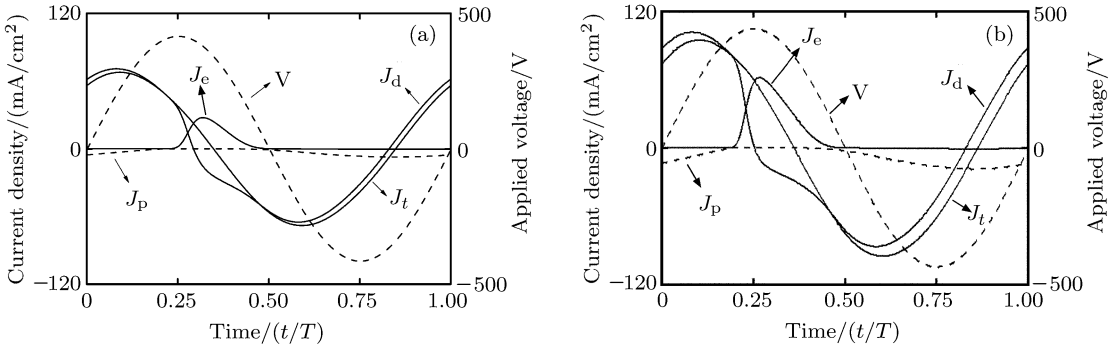



**Fig.4.** Time variations of the total current density $J_t$ and its components (displacement current density $J_d$, electron current density $J_c$, positive ion current density $J_p$) at the left electrode; (a) $\alpha$ mode, $V_{rf} = 415\,V$; (b) $\gamma$ mode, $V_{rf} = 436\,V$.

The spatial variations of the electric field, and electron and positive ion densities ($He^+$ and $He_2^+$) at four different moments of an rf cycle are shown in Fig.5.

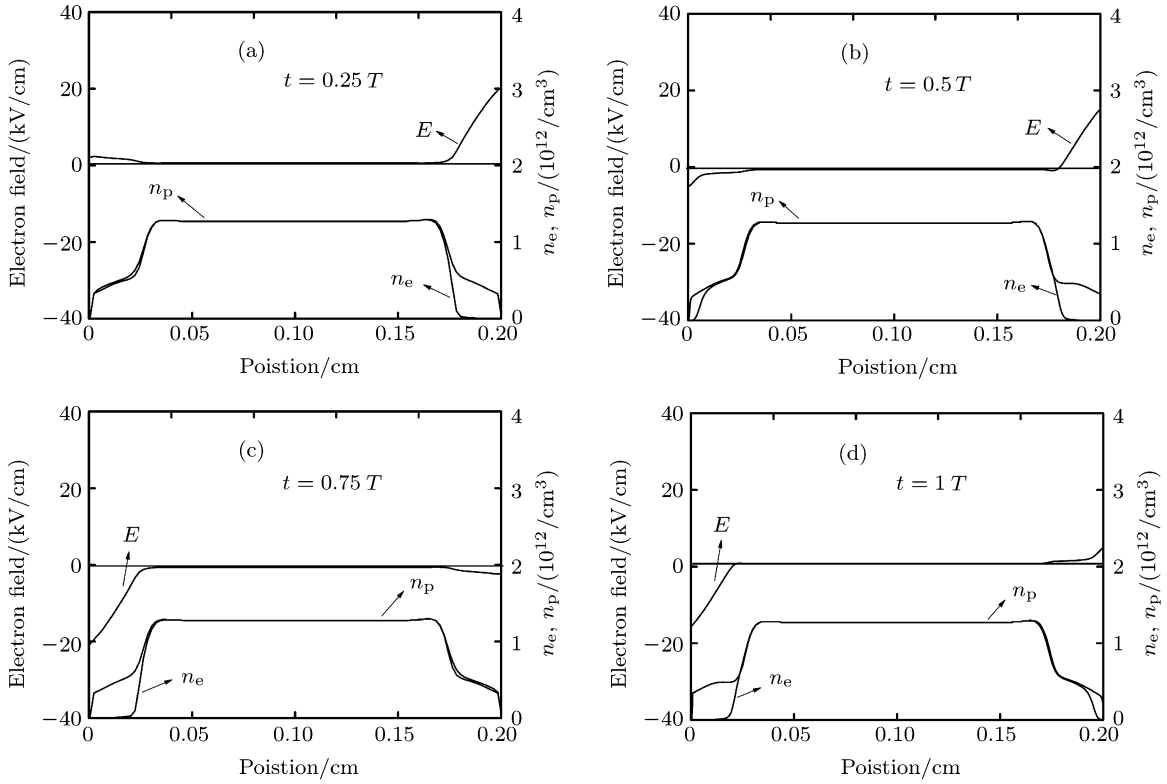



**Fig.5.** Spatial variations of the electric field and charged particle densities at four different moments of an rf cycle and a voltage amplitude of 436 V in the $\gamma$ mode.

As can be expected in the high frequency case, the ion density does not respond to the time-varying field and is sensitive only to the time-averaged field. More electrons are available in the momentary anode and when the applied voltage changes its sign, they flow to another electrode. During the anodic part of the cycle the plasma electrons move towards the electrode while the sheath contracts until some of these electrons are absorbed by the electrode. In the following sheath expansion the remaining electrons in the region close to the electrode are swept back to the plasma. If the frequency of sheath expansion is large enough, the electrons can gain energy from this expansion and ionize the gas molecules. There exists a stable homogeneous plasma between the two electrodes in our work. The plasma density is around $1.27 \times 10^{12}\,cm^{-3}$

with a sheath thickness maximum of 0.3 mm when the applied voltage amplitude is 436 V. The electrons are swept from the sheath into the plasma by the strong cathode electric field that could reach 30000 V/cm, whereas they flow to the electrode during the anodic part. The electric field in the sheath changes with a steep slope in the region close to the cathode as well as with a medium slope in the region close to the anode and stays invariably just about zero in the plasma.

The time averaged parts contributed to the electron energy balance in the discharge are shown in Fig.6.

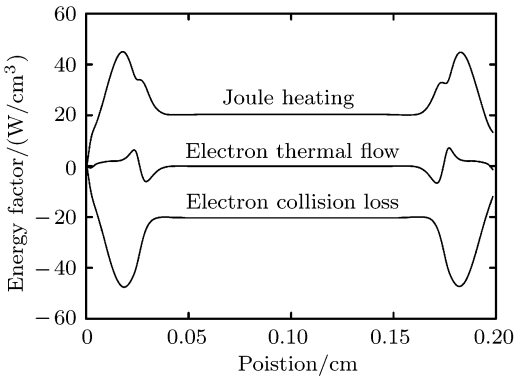



**Fig.6.** Time averaged contributions of Joule heating, electron thermal flow and collision loss to the electron energy balance in the discharge at a voltage amplitude of 436 V in the $\gamma$ mode.

The simulation results in Ref.[31] reveal the contributions of Joule heating, inelastic collisional loss/gain, and elastic collisional loss with a different electron energy conservation equation expression. In our model Joule heating plays a principal role in the electron energy impartation in the discharge and is dominant both in the sheath and the bulk plasma. On account of the strong electric field in the sheath, Joule Heating is carried into effect prominently in this sheath region. However, it drops in the region close to the electrode resulting from the weak electron flow in this area. The electron thermal flow is feeble compared with the Joule heating and the collision loss. The electron thermal flow can cause the electron energy to increase in the sheath because of the nonuniform energy distribution resulting from the sheath expansion and contraction. The collision loss contains the energy loss of the highly energetic electrons colliding with the cold background heavy species and the metastable particles. Due to the higher electron temperature in the sheath, more collisions take place there and the energy loss is especially serious in this region. The collision loss is balanced by Joule heating and electron thermal flow in the sheath as well as in the central region of two electrodes.

The spatial electron mean energies at different peak current densities[32,43] are presented in previous studies. However, the spatial–temporal variation in electron temperature needs to be described in a general form. Figure 7 shows the spatial–temporal variation in the $\gamma$ mode in our model. It can be seen that the electrons in the sheath have greater energy than those in the plasma. The maximal electron temperature in the sheath is 6.44 eV, while in the plasma it is a little more than 2 eV with a minimum of 2.02 eV. The electron temperature is much higher in cathode sheath than in anode sheath with a maximum of 2.96 eV. The sheath expansion provides the energy for the secondary electrons and the bulk electrons (electrons flow from the plasma to the electrode during the preceding sheath contraction, and they do not reach the electrode before the beginning of the sheath expansion), this property of rf discharges makes it more efficient to import energy to the plasma electrons than in dc discharges. There appears also a delay produced by the resistant part of the discharge gas.

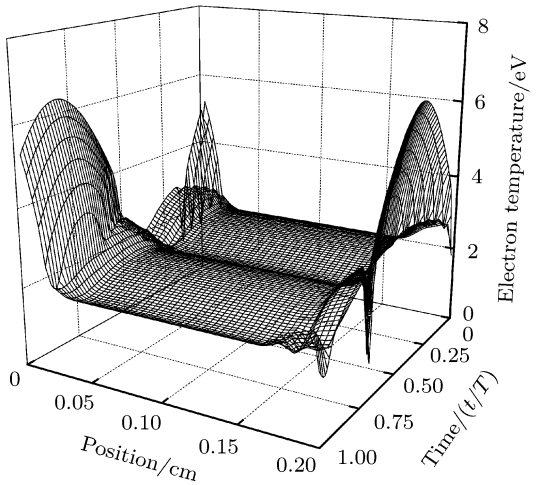



**Fig.7.** The spatial-temporal variation of the electron temperature at a voltage amplitude of 436 V in the $\gamma$ mode.

Figure 8 illustrates the electron source item in the $\gamma$ mode. This figure shows that a maximum electron flow occurs in the cathode sheath. As shown in Fig.8, the discharge appearing in the bulk plasma is tiny compared with that in the sheath due to the small electric field in the plasma. This figure also shows that the discharge spreads throughout the gap between the electrodes and especially is very strong in the sheath region. A majority of electrons are generated in the

sheath and then they are pushed to the central region of the electrodes and lose their energy gained from the sheath by collisions with the other species.

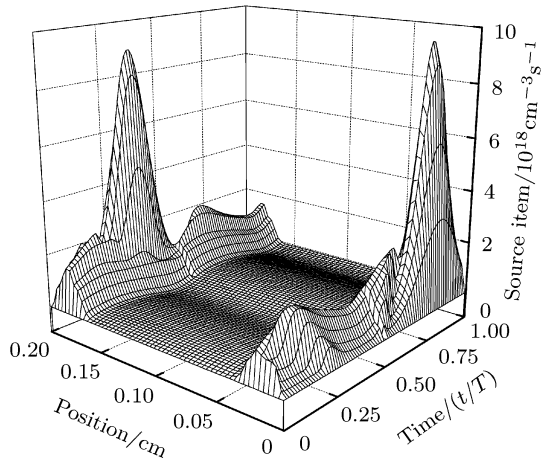



**Fig.8.** The spatial-temporal variation of the source item at a voltage amplitude of 436 V in the $\gamma$ mode.

### D. The effect of the secondary electron emission

The secondary electron emission is important in the $\gamma$ mode of a low pressure rf glow discharge,[29] and also in an atmospheric pressure rf glow discharge.[31,32] And the secondary electron regime occurs when the contribution of the cathode-emitted electrons to the total ionization becomes large. Figure 9 reveals the effects of secondary electrons in our model. When the emission coefficient is large, the density of the bulk plasma and the time averaged electron temperature increase. There are more electrons emitted from the cathode by the ion bombardment if the emission coefficient is greater. The electrons gain energy from the electric field in sheath, meanwhile the secondary electrons lose most of their energy in the sheath region. Then they penetrate into the plasma deeply. Actually, when the coefficient is below 0.05, the discharge current is not available in $\gamma$ mode of APGD, but they are in $\alpha$ mode. This could support the explanation that the secondary electron emission plays an important role in the $\gamma$ discharge mode. It also can be seen from the figure that there are fewer electrons present in the sheath region, but these electrons are possessed of the energy several times greater than that in the bulk plasma.

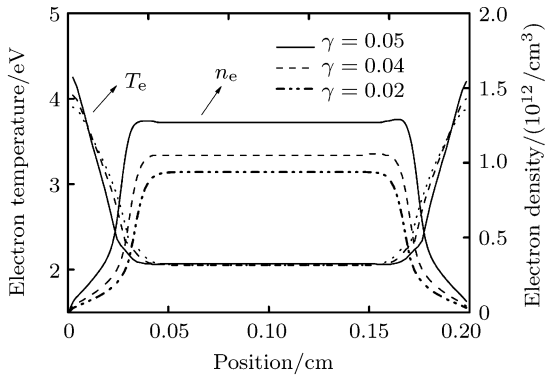



**Fig.9.** The time averaged electron density and electron temperature in the gap between the electrodes at different secondary electron emission coefficients and a voltage amplitude of 436 V.

## 4. Conclusions

There appear two discharge modes ($\alpha$ and $\gamma$) in an rf atmospheric pressure glow discharge just like those in an rf low pressure glow discharge. A self-consistent computational study is presented to investigate the discharge characteristics such as spatial structure of the discharge and the spatial–temporal electron temperature during the cycle using the existing theories of the rf capacitive discharge in the $\gamma$ mode of rf APGD between two metallic parallel planar electrodes. A steady discharge is achieved and the plasma density is $1.27 \times 10^{12}\,\mathrm{cm}^{-3}$ with an electron temperature of about 2 eV in the bulk plasma, along with a maximal electron temperature of 6.44 eV in the cathode sheath and 2.96 eV in the anode sheath, with a voltage amplitude of 436 V applied. The discharge current density amplitude is calculated to be $95\,\mathrm{mA/cm}^2$. The electrons gain the energy mainly from Joule heating, which takes place prominently in the sheath owing to a great electric field existing in this area, and the electron energy loss is especially serious also in the sheath due to the great collision rate caused by the high electron temperature there. It is also shown that the secondary electron emission plays an important role in the discharge by changing the emission coefficient. A higher plasma density and greater electron energy in the sheath region in the $\gamma$ mode give APGDs ample scope of applications.

# References


[1] Roth J R 1995 *Industrial Plasma Engineering*: *Principles* (Institute of Physics, Bristol)

[2] Lieberman M A and Lichtenberg A J 1994 *Principles of Plasma Discharge and Materials Processing* (Wiley, New York)

[3] Moravej M, Yang X, Nowling G R, Chang J P and Hicks R F 2004 *J. Appl. Phys.* **96** 7011

[4] Chen F F 1984 *Introduction to Plasma Physics and Controlled Fusion* (Plenum, New York)

[5] Fauchais P and Vardelle A 1997 *IEEE Trans. Plasma Sci.* **25** 1258

[6] Smith R W, Wei D and Apelian D 1989 *Plasma Chem. Plasma Process.* **9** 1358

[7] Goldman M and Sigmond R S 1982 *IEEE Trans. Electr. Insul.* **17** 90

[8] Chang J S, Lawless P A and Yammoto T 1991 *IEEE Trans. Plasma Sci.* **19** 1152

[9] Ramakrishnan S and Rogozinski M W 1997 *J. Phys.* D **30** 636

[10] Ramakrishnan S, Gershenzon M, Polivka F, Kearney T N and Rogozinski M W 1997 *IEEE Trans. Plasma Sci.* **25** 937

[11] Park Jaeyoung, Henins I, Herrmann H W, Selwyn G S and Hicks R F 2001 *J. Appl. Phys.* **89** 20

[12] Wang X X, L Z Z and Mao Y K 2002 *Acta Phys. Sin.* **51** 2778

[13] Wang Y H and Wang D Z 2003 *Acta Phys. Sin.* **52** 1694

[14] Wang Y H and Wang D Z 2005 *Acta Phys. Sin.* **54** 1295

[15] Dong L F, Mao Z G and Ran J X 2005 *Chin. Phys.* **14** 1618

[16] Roth J R 1995 *Industrial Plasma Engineering, Principles* Vol1 (Institute of Physics, Bristol) p453

[17] Kunhardt E E 2000 *IEEE Trans. Plasma Sci.* **28** 189

[18] Park J, Henins I, Herrmann H W, Selwyn G S, Jeong J Y, Hicks R F, Shim D and Chang C S 2000 *Appl. Phys. Lett.* **76** 288

[19] Stark R H and Schoenbach K H 1990 *J. Appl. Phys.* **85** 2075

[20] Kanazawa S, Kogoma M, Moriwaki T and Okazaki S 1988 *J. Phys.* D **21** 838

[21] Laroussi M, Alexeff I, Richardson J P and Dyer F F 2002 *IEEE Trans. Plasma Sci.* **30** 158

[22] Koinuma H, Ohkubo H, Hashimoto T, Inornata K, Shiraishi T, Miyanaga A and Hayashi S 1992 *Appl. Phys. Lett.* **60** 816

[23] Shenton M J and Stevens G C 2002 *IEEE Trans. Plasma Sci.* **30** 184

[24] Moisan M, Zakrzewski Z, Etmadi R and Rostaing J C 1998 *J. Appl. Phys.* **83** 5691

[25] Yatsenko N A 1981 *Zh. Tekh. Fiz.* **51** 1195

[26] He D and Hall D R 1984 *IEEE J. Quantum Electron.* **20** 509

[27] Hugel H E 1986 *Proc. SPIE* **650** 2

[28] Raizer Y P, Shneider M N and Yatsenko N A 1995 *Radio-Frequency Capacitive Discharge* (CRC, Boca Raton, FL)

[29] Belenguer P H and Boeuf J P 1990 *Phys. Rev.* A **41** 4447

[30] Park J, Henins I, Herrmann H W, Selwyn G S and Hicks R F 2001 *J. Appl. Phys.* **89** 20

[31] Yuan X and Raga L L 2003 *IEEE Trans. Plasma Sci.* **31** 495

[32] Shi J J and Kong M G 2005 *J. Appl. Phys.* **97** 023306

[33] Yang X, Moravej M, Nowling G R, Babayan S E, Panelon J, Chang J P and Hicks R F 2005 *Plasma Sources Sci. Technol.* **14** 314

[34] Golubovskii Yu B, Maiorov V A, Behnke J and Behnke J F 2003 *J. Phys.* D: *Appl. Phys.* **36** 39

[35] Golubovskii Yu B, Maiorov V A, Behnke J and Behnke J F 2002 *Proc. HAKONE VILL 8*$^{\text{th}}$ *Int. Symp. On High Pressure Low Temperature Plasma Chemistry* (Puhajarve, Estonia, 21-25 July) vol.1 48

[36] Ward A L 1962 *J. Appl. Phys.* **32** 2789

[37] Shon J W and Kushner M J 1994 *J. Appl. Phys.* **75** 1883

[38] Stevefelt J, Pouvesle J M and Bouchoule A 1982 *J. Chem.* **76** 4006

[39] Deloche R, Monchicourt P, Cheret M and Lambert F 1976 *Phys. Rew.* A **13** 1140

[40] Pouvesle J M, Bouchoule A and Stevefelt J 1982 *J. Chem. Phys.* **77** 817

[41] Brok W J M, Bowden M D, van Dijk J, van der Mullen J J M and Kroesen G M W 2005 *J. Appl. Phys.* **98** 013302

[42] Wang Y H and Wang D Z 2005 *Phys. Plasma* **12** 023503

[43] Shi J J and Kong M G 2005 *IEEE Trans. Plasma Sci.* **32** 624